# $\gamma$-ray spectroscopy of $^{33}$P and $^{33}$S after fusion-evaporation reactions

B. Fu,[1] M. Seidlitz,[1] A. Blazhev,[1] M. Bouhelal,[2] F. Haas,[3,4] P. Reiter,[1] K. Arnswald,[1] B. Birkenbach,[1] C. Fransen,[1] G. Friessner,[1] A. Hennig,[1] H. Hess,[1] R. Hirsch,[1] L. Lewandowski,[1] D. Schneiders,[1] B. Siebeck,[1] T. Steinbach,[1] T. Thomas,[1] A. Vogt,[1] A. Wendt,[1] K. Wolf,[1] and K. O. Zell[1]

[1]*Institut für Kernphysik, Universität zu Köln, D-50937 Cologne, Germany*
[2]*Laboratoire de Physique Appliquée et Théorique, Université Larbi Tébessa, Tébessa, Algeria*
[3]*Université de Strasbourg, IPHC, F-67037 Strasbourg, France*
[4]*CNRS, UMR7178, F-67037 Strasbourg, France*

(Received 18 May 2016; published 19 September 2016)

Excited states with intermediate and high spins in $^{33}$P and $^{33}$S have been populated using the $^{26}$Mg($^{13}$C,$npα$) and $^{26}$Mg($^{13}$C,$2nα$) fusion-evaporation reactions. The level schemes of both nuclei have been considerably extended. Utilizing $\gamma\gamma$ angular correlations the spin-parity assignment of the new excited states in $^{33}$P has been investigated. The experimentally determined results from both nuclei were compared to $0\hbar\omega$ and $1\hbar\omega$ truncated *p-sd-pf* shell-model calculations utilizing the PSDPF interaction, showing a very good agreement between experiment and theory.

DOI: 10.1103/PhysRevC.94.034318

## I. INTRODUCTION

The upper *sd*-shell nuclei are ideal test cases for shell-model calculations. The excitations of valence nucleons within the *sd* shell produce only positive-parity states, while excitations across the $N$ or $Z = 20$ shell gaps produce negative-parity intruder states. The universal *sd* interaction (USD) [1,2] and more recently the USDA and USDB [3] interactions have been quite successful in the description of the $0\hbar\omega$ states in *sd*-shell nuclei. In order to understand the intruder states with negative parity, several different interactions were developed and truncated *sd-pf* shell-model calculations were performed. Since shell-model calculations in the full proton and neutron *sdpf* model space are not possible due to the huge dimension of this configuration, the usual approach for neutron-rich *sd* nuclei is to limit the valence protons in the *sd* shell and to allow some neutrons to be excited from the *sd* shell into the *pf* shell or to have valence neutrons in the *pf* shell in case of neutron-rich isotopes with $N > 20$. Among the most used mixed *sd-pf* interactions are the SDPF-NR [4,5] and its more recent version SDPF-U [6], which describe very nicely the energy levels for very neutron-rich isotopes with $N > 20$ and $Z = 14$–$19$. Another interaction used for the $Z = 8$–$20$, $N = 18$–$25$ nuclei is the SDPFMW interaction [7]; its single-particle energies were adapted and the two-body matrix elements optimized for the $A \sim 30$ region. However, the above interactions do not describe successfully the odd-$A$ *sd*-shell nuclei. In particular, the calculated energies for the first negative-parity states are generally too high, and the spin order of negative-parity states can not be reproduced. For *sd*-shell nuclei close to $N = 20$ the description of the intruder states was not satisfying.

To overcome this issue, the PSDPF interaction [8] was derived. It describes both $0\hbar\omega$ positive-parity states and $1\hbar\omega$ negative-parity intruder states in the full *p-sd-pf* model space, with a $^4$He core allowing up to one neutron excitation between two major shells. The comparison between experiment and the *p-sd-pf* shell-model calculations shows good agreement [9–11]. In this work we present new experimental results and test the applicability of the PSDPF interaction to the $A = 33$ neutron-rich nuclei $^{33}$P and $^{33}$S.

Experimental investigations started in the 1970s, utilizing transfer reactions to establish the level scheme of $^{33}$P up to 6.2 MeV [12–16]. Wagner *et al.* [17] and Poletti *et al.* [16] measured the lifetime of low-lying states using the Doppler-shift attenuation method (DSAM). In 1987 Davis and Nelson determined levels with high excitation energies up to 10.12 MeV by the $^{30}$Si($\alpha,p$)$^{33}$P reaction [18]. In 2009 Chakrabarti *et al.* extended the level scheme up to 7.9 MeV utilizing the fusion-evaporation reaction $^{18}$O($^{18}$O,$p2n\gamma$)$^{33}$P [19].

The level scheme of $^{33}$S was established up to 7.9 MeV using particle-$\gamma$ coincidences [20–22]. By the means of particle spectroscopy, excitation energies of $^{33}$S were determined up to 17 MeV [23–25]. Further on, lifetime measurements in $^{33}$S for states with energies up to 5.3 MeV were determined by Carr *et al.* [26] using the reaction $^{30}$Si($\alpha,n\gamma$)$^{33}$S and DSAM. Recently, Bisoi *et al.* [27] studied $^{33}$S using the reaction $^{27}$Al($^{12}$C, $\alpha pn$)$^{33}$S. They extended the known level scheme up to 7.8 MeV, reporting three new transitions, and determined the lifetimes of the newly proposed high-spin $11/2^+$ and $15/2^-$ states by DSAM [27].

In the present work, intermediate- and high-spin states in $^{33}$P and $^{33}$S have been populated using the fusion-evaporation reactions $^{26}$Mg($^{13}$C,$npα$)$^{33}$P and $^{26}$Mg($^{13}$C,$2nα$)$^{33}$S, respectively. The level schemes of both nuclei have been extended to higher spins. In Sec. II the details about the experimental setup are described. The results of the data analysis are given in Sec. III. The shell-model calculations and comparison with experimental findings are discussed in Sec. IV. The paper concludes with a final summary in Sec. V.

## II. EXPERIMENTAL SETUP AND DATA ANALYSIS

Excited states of $^{33}$P with energies up to 10 MeV have been populated by the fusion-evaporation reaction $^{26}$Mg($^{13}$C,$npα$)$^{33}$P, employing a $^{13}$C beam delivered by the FN Tandem accelerator located at the Institute for Nuclear

 

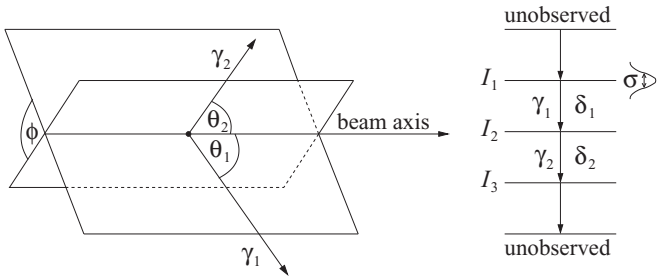


FIG. 1. Correlation of two coincident $\gamma$ rays. The $\gamma$-ray transitions are characterized by the multipole-mixing ratios $\delta_i$ and the levels by their spins $I_i$. The width of the alignment distribution is labeled with $\sigma$ (adapted from Ref. [35]).

Physics in Cologne. At the beam energy of 46 MeV, the program CASCADE [28] yielded a cross section of around 120 mb for the population of the $np\alpha$ reaction channel. The $^{26}$Mg target with a thickness of 0.22 $\frac{\text{mg}}{\text{cm}^2}$ was coated on a 66 $\frac{\text{mg}}{\text{cm}^2}$ thick Bi backing with an additional 1 $\frac{\text{mg}}{\text{cm}^2}$ In layer plus an 108 $\frac{\text{mg}}{\text{cm}^2}$ thick Cu layer for heat dissipation. Recoiling residual nuclei were stopped after the reaction inside the Bi backing. De-excitation $\gamma$ rays of excited states in $^{33}$P and $^{33}$S were detected with the High-efficiency Observatory for $\gamma$-Ray Unique Spectroscopy (HORUS) [29]. The 14 high-purity germanium (HPGe) detectors of the HORUS array, six of them equipped with BGO shields, were placed in close geometry around the target chamber at distances of around 10 cm from the target position and at angles of 35°, 45°, 90°, 135°, and 145° with respect to the beam axis. Thus, the solid-angle coverage was about 40% of $4\pi$. $\gamma$-ray energies were calibrated using a $^{226}$Ra source. The absolute $\gamma$-ray efficiency was determined to be 1.8% at an energy of 1.3 MeV. During the experiment, the count rate of each individual HPGe crystal was maintained between 9 and 12 kHz. $\gamma\gamma$ coincidences were recorded utilizing the XIA Digital Gamma Finder (DGF) data-acquisition system [30] and were analyzed using the programs SOCO [31] and TV [32]. The recorded $\gamma$ rays were sorted into three different kinds of $\gamma\gamma$-coincidence matrices: (i) a symmetrical general matrix to study $\gamma\gamma$-coincidence relations; (ii) 17 angular-correlation-group matrices, corresponding to the relative angles $\theta_{1,2}$ and $\phi$ between all detector pairs, to investigate spins and parities of the observed levels; and (iii) five matrices according to the angle $\theta$ to determine level lifetimes using DSAM.

The unknown spins and parities of excited states were investigated employing the $\gamma\gamma$ angular-correlation method. Using the phase convention of Krane, Steffen, and Wheeler [33,34] the angular distribution of two $\gamma$ rays emitted in coincidence by the recoil nucleus can be described by the following formula (cf. Fig. 1 for definitions):

$$W(\theta_1,\theta_2,\phi) = \sum_{k,k_1k_2} B_{k_1}(I_1) A_k^{k_1k_2}(\gamma_1) A_{k_2}(\gamma_2) H_{kk_1k_2}(\theta_1,\theta_2,\phi). \quad (1)$$

The statistical tensor $B_{k_1}(I_1)$ describes the initial orientation of the recoiling nucleus. The correlation coefficients $A_k^{k_1k_2}$ and $A_{k_2}$ depend on the spins $I_i$ and the multipole-mixing ratios $\delta_i$ of the involved levels and transitions. $H_{kk_1k_2}(\theta_1,\theta_2,\phi)$ is the function of angular correlation, depending on the angles $\theta_1$, $\theta_2$, and $\phi$.

Regarding to these angles, all possible combinations of two detectors of the HORUS array were arranged in 17 angular-correlation groups, each one characterized by its values for $\theta_1$, $\theta_2$, and $\phi$. Using the code CORLEONE [36], the angular distribution function $W(\theta_1,\theta_2,\phi)$ of two coincident $\gamma$-ray transitions was fitted to the measured $\gamma$-ray intensities in the $\gamma\gamma$ matrix of the corresponding correlation group. Applying this method to all correlation groups, it was possible to test different spin and parity assignments for the levels involved. The results of the analysis are described in the following sections.

## III. EXPERIMENTAL RESULTS

The $\gamma$-ray transitions of the nuclei $^{33}$P and $^{33}$S were investigated by means of $\gamma\gamma$-coincidence data. A total number of $2.0 \times 10^9$ prompt coincident $\gamma$-ray events were recorded, which allowed for identification even of weak $\gamma$-ray transitions and their unambiguous allocation in the level scheme up to excitation energies of about 10 MeV. Thus, it was possible to establish several new $\gamma$-ray transitions and energy levels and to extend the level schemes of both nuclei. Additionally, spins of several states were determined by means of $\gamma\gamma$ angular correlations. The experimentally deduced energies, spins, and parities of the levels as well as the relative intensities of the de-exciting $\gamma$-ray transitions are summarized in Table I.

### 1. $^{33}$P

Chakrabarti *et al.* established the level scheme of $^{33}$P up to 8 MeV using the fusion-evaporation reaction $^{18}$O($^{18}$O ,$2np$)$^{33}$P at 34 MeV [19]. The previously reported $\gamma$-ray transitions at 1028, 1298, 2142, and 3605 keV were confirmed to belong to $^{33}$P in the present analysis. However, some of these transitions needed to be relocated in the level scheme due to $\gamma\gamma$-coincidence relations, thus yielding modifications of the corresponding excited states at 3990 and 7966 keV, which were introduced by Chakrabarti *et al.* Figures 2(a)–2(c) show $\gamma$-ray spectra in coincidence with the 1028-, 2142-, and 1298-keV $\gamma$-ray transitions, respectively. Obviously, the 2142-keV $\gamma$-ray transition is coincident with the transitions at 1028, 1298, 1412, 1848, and 2378 keV, and thus it cannot be in parallel to any of these transitions. Furthermore, new $\gamma$-ray transitions at 880, 1168, 1349, 1484, 1535, 2090, 2271, 2581, 2762, 3169, 3440, 3587, and 4467 keV were found to de-excite levels above 6 MeV. These transitions were placed in the level scheme according to the observed $\gamma\gamma$-coincidence relations, energy sums, and intensity balances [cf. Fig. 2(d)].

The energy sums of the 1028- plus 2142-keV transitions and of the 1298- plus 2142-keV transitions matched the energies of the 3169- and 3440-keV transitions, respectively. Hence, the 2142-keV transition had to be placed in between the de-exciting 1028- and 1298-keV transitions, introducing new energy levels at 9078 and 10106 keV. Moreover, the newly established energy level at 9078 keV is de-excited by

TABLE I. Level energies, spin-parity assignments, $\gamma$-ray transition energies, branching ratios, and multipolarities for $^{33}$P and $^{33}$S. The energies of $\gamma$-ray transitions, branching ratios, and level spin-parity assignments are determined from the present experiment. The transition multipolarities are taken from the National Nuclear Data Center (NNDC) [38].

| $E_i$ (keV) | $E_f$ (keV) | $J_i^\pi$ | $J_f^\pi$ | $E_\gamma$ (keV) | Branching ratios (%) | Multipolarity |
|---|---|---|---|---|---|---|
| | | | $^{33}$P | | | |
| 1432 | 0 | $3/2^+$ | $1/2^+$ | 1431.6 (3) | 100.0 (10) | $M1+E2$ |
| 1848 | 0 | $5/2^+$ | $1/2^+$ | 1847.5 (3) | 100.0 (5) | $E2+M3$ |
| | 1432 | $5/2^+$ | $3/2^+$ | 415.9 (2) | 7.0 (1) | $M1+E2$ |
| 3491 | 0 | $5/2^+$ | $1/2^+$ | 3490.1 (10) | 13.4 (15) | $E2(+M3)$ |
| | 1432 | $5/2^+$ | $3/2^+$ | 2058.5 (8) | 73.6 (25) | $(M1+E2)$ |
| | 1848 | $5/2^+$ | $5/2^+$ | 1642.6 (4) | 100.0 (22) | $M1(+E2)$ |
| 3628 | 1432 | $7/2^+$ | $3/2^+$ | 2196.0 (8) | 100.0 (48) | $E2$ |
| | 1848 | $7/2^+$ | $5/2^+$ | 1780.1 (6) | 44.5 (45) | $M1(+E2)$ |
| 4226 | 1432 | $7/2^-$ | $3/2^+$ | 2794.1 (13) | 1.2 (2) | $(M2)$ |
| | 1848 | $7/2^-$ | $5/2^+$ | 2378.2 (5) | 100.0 (4) | $E1(+M2)$ |
| | 3491 | $7/2^-$ | $5/2^+$ | 735.6 (3) | 8.9 (2) | $E1$ |
| 5453 | 1848 | $9/2^-$ | $5/2^+$ | 3604.5 (15) | 1.3 (4) | $(M2)$ |
| | 3628 | $9/2^-$ | $7/2^+$ | 1824.4 (4) | 8.7 (2) | $(E1)$ |
| | 4226 | $9/2^-$ | $7/2^-$ | 1226.3 (3) | 100.0 (3) | $M1+E2$ |
| 5638 | 5453 | $11/2^-$ | $9/2^-$ | 185.6 (3) | 79.9 (18) | $M1$ |
| | 4226 | $11/2^-$ | $7/2^-$ | 1411.9 (4) | 100.0 (23) | $E2$ |
| 6518 | 5638 | | $11/2^-$ | 880.3 (12) | 100.0 (70) | |
| 6807 | 4226 | (7/2,9/2,11/2) | $7/2^-$ | 2581.6 (10) | 19.6 (50) | |
| | 5638 | (7/2,9/2,11/2) | $11/2^-$ | 1168.6 (8) | 100 (11) | |
| 6936 | 5453 | (9/2, 13/2) | $9/2^-$ | 1484.2 (9) | 13.8 (29) | |
| | 5638 | (9/2, 13/2) | $11/2^-$ | 1297.9 (4) | 100.0 (31) | $(Q)$ |
| 6988 | 4226 | (7/2,9/2,11/2) | $7/2^-$ | 2761.0 (11) | 100 (11) | |
| | 5453 | (7/2,9/2,11/2) | $9/2^-$ | 1535.4 (11) | 36.3 (71) | |
| | 5638 | (7/2,9/2,11/2) | $11/2^-$ | 1349.4 (10) | 49 (10) | |
| 9078 | 5638 | (7/2,11/2,15/2) | $11/2^-$ | 3440 (2) | 25.3 (25) | |
| | 6807 | (7/2,11/2,15/2) | (7/2,9/2,11/2) | 2269.8 (12) | 18.9 (29) | |
| | 6936 | (7/2,11/2,15/2) | (9/2, 13/2) | 2141.8 (7) | 100.0 (35) | |
| | 6988 | (7/2,11/2,15/2) | (7/2,9/2,11/2) | 2090.6 (5) | 50.3 (29) | |
| 10106 | 5638 | (5/2,9/2,13/2,17/2) | $11/2^-$ | 4468 (3) | 5.7 (11) | |
| | 6518 | (5/2,9/2,13/2,17/2) | | 3587 (2) | 13.4 (17) | |
| | 6936 | (5/2,9/2,13/2,17/2) | (9/2, 13/2) | 3169.4 (12) | 19.4 (15) | |
| | 9078 | (5/2,9/2,13/2,17/2) | (7/2,11/2,15/2) | 1027.6 (3) | 100.0 (18) | $(D)$ |
| | | | $^{33}$S | | | |
| 841 | 0 | $1/2^+$ | $3/2^+$ | 840.6 (6) | 100 (4) | $M1+E2$ |
| 1967 | 0 | $5/2^+$ | $3/2^+$ | 1966.9 (4) | 100.0 (2) | $M1+E2$ |
| | 841 | $5/2^+$ | $1/2^+$ | 1126.3 (7) | 1.5 (1) | $E2$ |
| 2935 | 0 | $7/2^-$ | $3/2^+$ | 2934.4 (8) | 90.1 (11) | $(M2+E3)$ |
| | 1967 | $7/2^-$ | $5/2^+$ | 967.5 (4) | 100.0 (7) | $E1(M2)$ |
| 2969 | 0 | $7/2^+$ | $3/2^+$ | 2968.9 (12) | 100.0 (22) | $E2$ |
| | 1967 | $7/2^+$ | $5/2^+$ | 1002.0 (8) | 13.1 (18) | $M1(+E2)$ |
| 4049 | 1967 | $9/2^+$ | $5/2^+$ | 2081.5 (6) | 100.0 (31) | $E2(+M3)$ |
| | 2935 | $9/2^+$ | $7/2^-$ | 1113.6 (10) | 6.1 (1.9) | $E1$ |
| | 2969 | $9/2^+$ | $7/2^+$ | 1079.5 (8) | 32.8 (25) | $(M1+E2)$ |
| 4095 | 1967 | $7/2^+$ | $5/2^+$ | 2128.2 (11) | 100 (9) | $(M1+E2)$ |
| 4730 | 2935 | $9/2^-$ | $7/2^-$ | 1795 (2) | 20.3 (29) | $M1+E2$ |
| | 2969 | $9/2^-$ | $7/2^+$ | 1760.9 (11) | 100.0 (39) | $E1(+M2)$ |
| 4867 | 2935 | $11/2^-$ | $7/2^-$ | 1932.1 (10) | 100 (8) | $(E2(+M3))$ |
| 5480 | 2935 | | $7/2^-$ | 2545 (2) | 70.1 (72) | |
| | 2969 | | $7/2^+$ | 2510.5 (12) | 100 (8) | |
| | 4095 | | $7/2^+$ | 1383.7 (10) | 29.2 (61) | |
| 5793 | 4730 | | $9/2^-$ | 1063.4 (8) | 100 (5) | |
| 7000 | 4049 | | $9/2^+$ | 2951.3 (12) | 100 (6) | |
| | 4730 | | $9/2^-$ | 2269.9 (10) | 84.4 (61) | |
| | 4867 | | $11/2^-$ | 2133.2 (11) | 71.5 (68) | |

TABLE I. (*Continued.*)

| $E_i$ (keV) | $E_f$ (keV) | $J_i^\pi$ | $J_f^\pi$ | $E_\gamma$ (keV) | Branching ratios (%) | Multipolarity |
|---|---|---|---|---|---|---|
| | 5480 | | $1/2^+$ | 1520.3 (8) | 82.3 (58) | |
| 7180 | 4867 | $(11/2^+)$ | $11/2^-$ | 2313 (2) | 100 (8) | |
| 7820 | 4867 | $15/2^-$ | $11/2^-$ | 2954 (3) | 100 (7) | $(M1+E2)$ |
| 8641 | 5793 | | | 2847 (3) | 6.9 (28) | |
| | 7000 | | | 1641.4 (16) | 100 (6) | |
| 9814 | 8641 | | | 1173.2 (8) | 100 (7) | |

three more $\gamma$-ray transitions at 2090, 2271, and 3440 keV. Due to $\gamma\gamma$-coincidence relations and energy sums of the 2090-keV transition and the $\gamma$-ray transitions at 186, 1227, 1349, 1412, 1535, and 2762 keV, another energy level was firmly established at 6988 keV. The known energy level at 6936 keV was found to be de-excited by an additional 1484-keV transition to the $9/2^-$ level. A new energy level at 6807 keV was introduced due to the observation of a 2271-keV populating transition and two weak de-exciting $\gamma$-ray transitions at 1168 and 2581 keV. The $\gamma\gamma$-coincidence

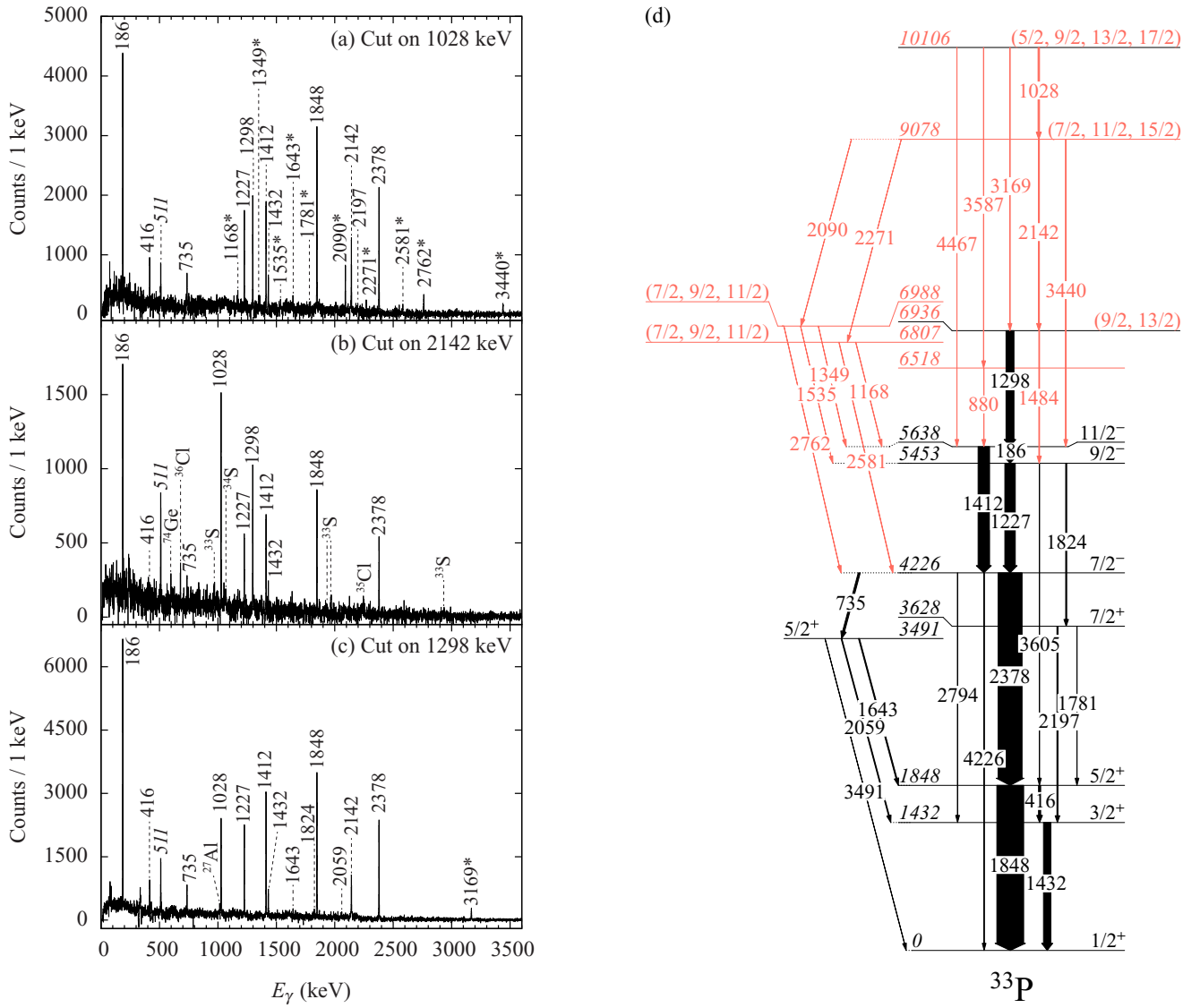


FIG. 2. $\gamma\gamma$-coincidence spectra with gates on $\gamma$-ray transitions at (a) 1028, (b) 2142, and (c) 1298 keV in $^{33}$P, respectively. The newly detected $\gamma$ rays are indicated with an asterisk. (d) Partial level scheme of $^{33}$P, as observed in the current experiment. New energy levels and assigned $\gamma$-ray transitions are marked in red. The widths of the arrows correspond to the relative intensities of the observed $\gamma$-ray transitions.

analysis showed that the $\gamma$-ray events detected at 1356 keV, correspond only to the double-escape events of the 2378-keV transition, and not a possible transition between the 6807- and the 5453-keV levels. The newly found $\gamma$-ray transitions at 880, 3587, and 4467 keV were identified as new de-excitation paths off the 10106-keV level, with the cascade 3587+880 keV proceeding via a new level at 6518 keV [see Fig. 2(d)].

Additionally, it was possible to investigate spins of energy levels in $^{33}$P by means of $\gamma\gamma$ angular correlations. Using the program CORLEONE [36], the angular distribution function $W(\theta_1,\theta_2,\phi)$ of two coincident $\gamma$-ray transitions was fitted to the measured $\gamma$-ray intensities in the $\gamma\gamma$ matrix of each of the 17 angular-correlation groups, as described in Sec. II. With this method, spins and parities of the yrast band built on the $1/2^+$ ground state [18] were confirmed up to the $11/2^-$ state [cf. Figs. 3(a) and 3(b)]. For higher-lying states Chakrabarti *et al.* already showed that the 1028- and 1298-keV transitions are of dipole and quadrupole character, respectively, using a linear polarization measurement [19]. However, the spin and parity assignments of the corresponding energy levels were only tentative in that work: $(15/2^-)$ for the 6936-keV state (de-excited by a 1298-keV $\gamma$ ray) and $(17/2^+)$ for the 7966-keV state (de-excited by a 1028-keV $\gamma$ ray). Figures 3(c) and 3(d) show the experimentally deduced intensity distribution for the coincident $\gamma$ rays at 1298 and 1412 keV, measured in the present experiment, compared to calculated values for different scenarios of the spin and parity of the 6936-keV state. Obviously, a pure $E2$ transition with 1298 keV does not fit the experimental data [cf. Fig. 3(c)], which excludes both the option of a $7/2^-$ and a $15/2^-$ for the state at 6936 keV. Based on the present experimental data, we cannot decide whether the 1298-keV transition is parity changing or not. Nevertheless the angular-correlation analysis including multipole mixing fits well the experimental data [cf. Fig. 3(d)], assuming 9/2 or 13/2 spin for the 6936-keV state. A hypothesis of a 9/2 state gives the best results with a dominating quadrupole contribution ($\delta = 9.9(42)$) for the $9/2 \rightarrow 11/2^-$ transition, whereas a 13/2 state yields a mixing ratio of $\delta = -18(10)$. Using the same method, the spins of the newly established excited states at 9078 and 10106 keV were also determined, as shown in Figs. 3(e) and 3(f). With a spin assignment of $J = 9/2$ for the 6936-keV state, the spins of the 9078- and the 10106-keV states are limited to (7/2, 11/2) and (5/2, 9/2, 13/2), respectively. With $J = 13/2$ for the 6936-keV state, the spins of 9078- and 10106-keV states are limited to (11/2, 15/2) and (9/2, 13/2, 17/2), respectively. Thus, the combined possibilities for the spins of the 9078- and the 10106-keV states based on the current experimental analysis are $J = (7/2,11/2,15/2)$ and $J = (5/2,9/2,13/2,17/2)$, correspondingly.

For the weakly populated excited states at 6518, 6807, and 6988 keV, no accurate analysis of the $\gamma\gamma$ angular correlations was possible due to limited statistics. Nevertheless, the spin of the 6988 keV level could be restricted to (7/2,9/2,11/2) due to the three observed depopulating $\gamma$-ray transitions feeding the well-established $7/2^-$, $9/2^-$, and $11/2^-$ states. The same argument applies to the 6807-keV state, for which the depopulating transitions to the $7/2^-$ and $11/2^-$ states were recorded. Thus, the 6807-keV level can be ruled out as the $5/2^+$ state, reported by Khan *et al.* [37] at an excitation energy of 6820(60) keV, for which an $E3$ transition to the well-established $11/2^-$ state would compete with an $E1$ transition to the $7/2^-$ state.

We would also like to note that the energy level at 6940(150) keV with $J^\pi = (5/2,7/2)$, reported by Davis and Nelson [18], cannot be assigned clearly to a state observed in the present work. On the other hand, Davis and Nelson [18] have also reported an excited state at 10 120(150) keV, with a spin assignment of (1/2 to 13/2), which is likely to be identical with the newly established state at 10106 keV with $J = (5/2,9/2,13/2,17/2)$.

Table I, as well as the level scheme presented in Fig. 2(d), summarizes the experimental results for $^{33}$P deduced in the present experiment.

### 2. $^{33}$S

For $^{33}$S several new $\gamma$-ray transitions were detected, which de-excite states at excitation energies up to 10 MeV. Figures 4(a)–4(c) show the $\gamma\gamma$-coincidence spectra with gates on the 1520-, 1641-, and 1761-keV transitions, respectively. The present data reveal new $\gamma$-ray transitions for $^{33}$S at 1063, 1173, 1385, 1520, 1641, 2133, 2270, 2511, 2545, 2848, 2905, and 2951 keV. Coincidence relations as well as energy sums and intensity balances were used to place these $\gamma$-ray transitions in the level scheme of $^{33}$S, as shown in Fig. 4(d). The experimental results for $^{33}$S are summarized in Table I.

The new $\gamma$-ray transition observed at 2951 keV is in coincidence with $\gamma$ rays at 1079, 1967, 2081, and 2969 keV. The latter transitions are known as part of the de-excition cascade of the $9/2^+$ state at 4049 keV. Thus, the 2951-keV transition was placed on top of the $9/2^+$ state, depopulating a level at 7000 keV. Additionally, the level at 7000 keV is connected to the known $7/2^+$ state at 4095 keV, to the $9/2^-$ state at 4730 keV, and to the $11/2^-$ state at 4867 keV via the $\gamma$-ray transitions with energies of 2905, 2270, and 2133 keV, respectively. All de-exciting $\gamma$-ray transitions of the 7000-keV level were observed without significant Doppler broadening. Hence, with a typical stopping time $\Delta t_{\text{stop}} \sim 1.3$ ps of the recoils in the Bi backing of the target, a lifetime $> 1$ ps for the 7000-keV level is expected. Another de-excitation path was found via the 1520-keV transition feeding a new state at 5480 keV, which de-excites via the newly observed $\gamma$-ray transitions at 2511 and 2545 keV to the $7/2^+$ and $7/2^-$ states, respectively. This level cannot be the $1/2^+$ state, previously reported at the same energy in $(n,\gamma)$ [22], $(^3\text{He},p\gamma)$ [39], and $(^3\text{He},\alpha\gamma)$ reactions [21], as the direct $\gamma$-ray transitions to the ground and lowest-lying states, observed with a dominant branching in the aforementioned experiments, were missing in the present experiment. However, Dubois *et al.* observed additional weak $\gamma$-ray transitions at energies of 1.95, 2.53, and 2.95 MeV, in $^{34}$S$(^3\text{He},\alpha\gamma)^{33}$S reactions [21], which are—within the resolution of the formerly used NaI(Tl) crystals—consistent with the $\gamma$-ray decay of the newly proposed level at 5480 keV. In coincidence with all transitions depopulating the 7000-keV level, a strong $\gamma$-ray transition was observed at 1641 keV and was assigned to be a feeding transition to the 7000-keV level, thus introducing a new level with an excitation energy of

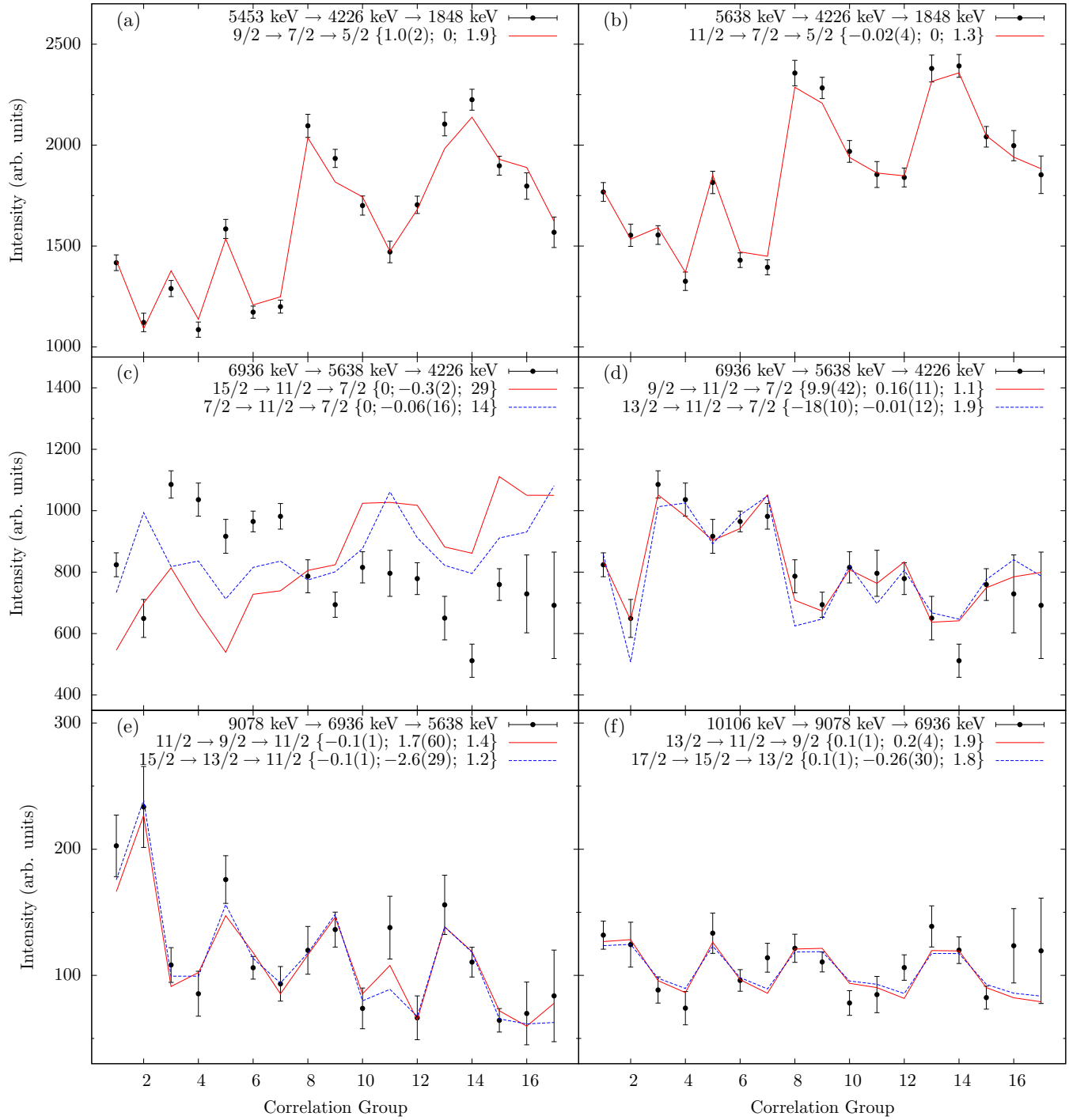


FIG. 3. $\gamma\gamma$ angular correlations for several coincident $\gamma$ rays in $^{33}$P. Experimental values are compared to calculations using the code CORLEONE. Additional information on deduced multipole-mixing ratios are given as well as the quality of the fit: $\{\delta_1; \delta_2; \chi^2\}$. Panels (a) and (b) show the results for the known $\gamma$-ray cascades from the $9/2^-$ state down to the $5/2^+$ state and from the $11/2^-$ state down to the $5/2^+$ state, respectively, reproducing known mixing ratios. Panel (c) shows the calculations for a pure *E2* transition from the 6936-keV state with spin 15/2 (solid line) and 7/2 (dashed line). These calculations do not reproduce the experimental data. For panel (d) multipole mixing for the 1298-keV transition is included, with a dominating quadrupole term. The calculations reproduce the experimental data. Results for the de-excitation of the higher-lying state at 9078 keV are shown in panel (e), exemplarily for a $11/2 \rightarrow 9/2 \rightarrow 11/2^-$ cascade (solid line) and a $15/2 \rightarrow 13/2 \rightarrow 11/2^-$ cascade (dashed line). Calculations for the state at 10106 keV are given in panel (f), showing the results for spin hypotheses of 13/2 (solid line) and 17/2 (dashed line).

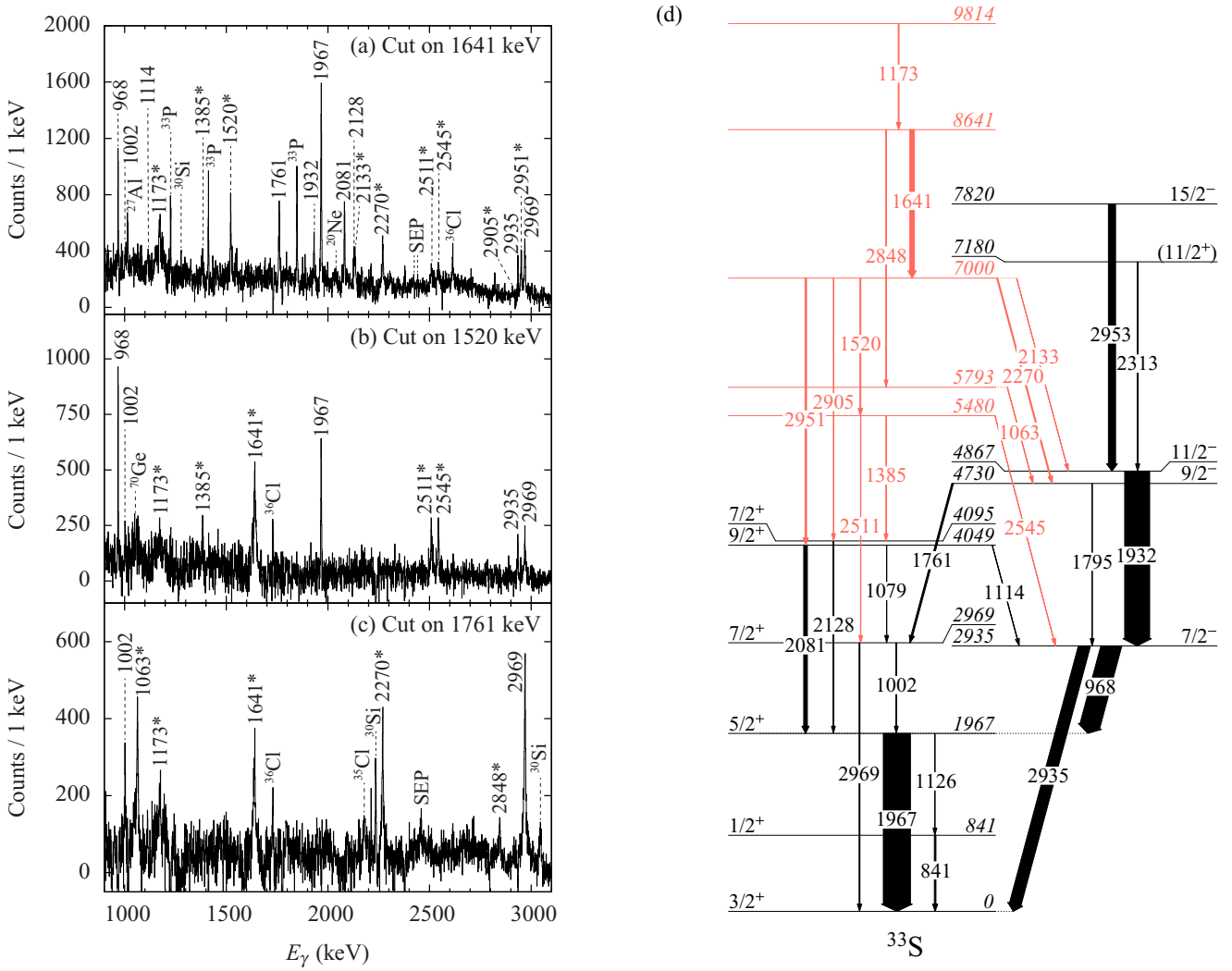


FIG. 4. $\gamma\gamma$-coincidence spectra with gates on $\gamma$-ray transitions at (a) 1641, (b) 1520, and (c) 1761 keV, respectively. The newly detected $\gamma$ rays are indicated with an asterisk. (d) Partial level scheme of $^{33}$S, as observed in the current experiment. New energy levels and assigned $\gamma$-ray transitions are marked in red. The widths of the arrows correspond to the relative intensities of the observed $\gamma$-ray transitions.

8641 keV. Due to observed Doppler-shift attenuation effects of the measured 1641-keV transition, the lifetime of the 8641-keV level should be $<1$ ps. Another weak decay branch of this level was observed via the 2848-keV $\gamma$ ray, which populates a new level at 5793 keV. Thus, the 8641-keV level is not assigned to the known $1/2^+$ state at 8640 keV, for which other strong de-exciting $\gamma$-ray transitions were known from previous experiments, based on the $^{32}$S$(n,\gamma)^{33}$S reaction [39]. Furthermore a high-lying state with excitation energy of 9814 keV was determined to be connected by a 1173-keV transition to the 8641-keV state. Additionally, $\gamma$-ray decay of the short-lived $(11/2^+)$ and $15/2^-$ states at 7180 and 7820 keV, respectively, reported recently by Bisoi *et al.* [27], was observed. However, the proposed 2450-keV transition de-exciting the $(11/2^+)$ state [27] could not be confirmed in the present experiment.

Within the present experiment it was not possible to perform $\gamma\gamma$ angular-correlation measurements for $^{33}$S due to the limited statistics. Thus, the spin and parity of the newly determined states were not assigned [see level scheme in Fig. 4(d)], while the spins and parities of the known states were taken from Refs. [27,38].

## IV. SHELL-MODEL CALCULATIONS AND DISCUSSION

The new experimentally obtained level schemes of $^{33}$P and $^{33}$S are compared to *p-sd-pf* shell-model calculations, which use the PSDPF [8] interaction to describe the $0\hbar\omega$ and $1\hbar\omega$ states in the model space. Based on a $^4$He core and using the full *p-sd-pf* model space, the PSDPF was constructed starting from primary interactions. For the nuclei nearby the upper *sd*-shell closure, these primary interactions were USDB [3] for *sd* major-shell and SDPF-NR [4,5] for *pf*-shell and *sd-pf* cross-shell terms. In addition, the matrix elements were tuned to reproduce experimental excitation energies [8].

In Tables II and III a comparison between experimentally known and corresponding shell-model states for $^{33}$P and $^{33}$S is made. In addition a more refined comparison between

TABLE II. Comparison between experimentally known states and calculated states in $^{33}$P. Further details are given in the text.

| Experiment | | PSDPF | | $E_{exp.} - E_{theo.}$ |
|---|---|---|---|---|
| $E_x$ (keV) | $J^\pi$ | $E_x$ (keV) | $J^\pi$ | $\Delta E$ (keV) |
| | | $^{33}$P | | |
| 0 | $1/2^+_{g.s.}$ | 0 | $1/2^+_{g.s.}$ | – |
| 1432 | $3/2^+$ | 1441 | $3/2^+_1$ | −9 |
| 1848 | $5/2^+$ | 1905 | $5/2^+_1$ | −57 |
| 2538 | $3/2^+$ | 2679 | $3/2^+_2$ | −141 |
| 3275 | $3/2^+$ | 3433 | $3/2^+_3$ | −158 |
| 3490 | $5/2^+$ | 3508 | $5/2^+_2$ | −18 |
| 3628 | $7/2^+$ | 3778 | $7/2^+_1$ | −150 |
| 4048 | $5/2^+$ | 3971 | $5/2^+_3$ | 77 |
| 4226 | $7/2^-$ | 4470 | $7/2^-_1$ | −244 |
| 5049 | $5/2^+$ | 5012 | $5/2^+_4$ | 37 |
| 5453 | $9/2^-$ | 5696 | $9/2^-_1$ | −244 |
| 5638 | $11/2^-$ | 5812 | $11/2^-_1$ | −180 |
| 5674 | $1/2^+$ | 5830 | $1/2^+_3$ | −156 |
| 6432 | $5/2^+$ | 6535 | $5/2^+_5$ | −100 |
| 6820 | $5/2^+$ | 6721 | $5/2^+_6$ | 99 |
| | | 6858 | $5/2^+_7$ | −38 |
| 6936 | (9/2,13/2) | 6720 | $9/2^-_3$ | 216 |
| | | 7109 | $9/2^+_3$ | −173 |
| | | 7222 | $13/2^-_1$ | −286 |
| 7146 | $5/2^+$ | 7172 | $5/2^+_8$ | −26 |

TABLE III. Comparison between experimentally known states and calculated states in $^{33}$S. For further information, see the text.

| Experiment | | PSDPF | | $E_{exp.} - E_{theo.}$ |
|---|---|---|---|---|
| $E_x$ (keV) | $J^\pi$ | $E_x$ (keV) | $J^\pi$ | $\Delta E$ (keV) |
| | | $^{33}$S | | |
| 0 | $3/2^+_{g.s.}$ | 0 | $3/2^+_{g.s.}$ | – |
| 841 | $1/2^+$ | 809 | $1/2^+_1$ | 32 |
| 1967 | $5/2^+$ | 1897 | $5/2^+_1$ | 70 |
| 2313 | $3/2^+$ | 2297 | $3/2^+_2$ | 16 |
| 2868 | $5/2^+$ | 2801 | $5/2^+_2$ | 67 |
| 2935 | $7/2^-$ | 2848 | $7/2^-_1$ | 87 |
| 2969 | $7/2^+$ | 3096 | $7/2^+_1$ | −127 |
| 3221 | $3/2^-$ | 3034 | $3/2^-_1$ | 187 |
| 3832 | $5/2^+$ | 3690 | $5/2^+_3$ | 142 |
| 3935 | $3/2^+$ | 3617 | $3/2^+_3$ | 318 |
| 4048 | $9/2^+$ | 4111 | $9/2^+_1$ | −63 |
| 4055 | $1/2^+$ | 3850 | $1/2^+_2$ | 205 |
| 4095 | $7/2^+$ | 4019 | $7/2^+_2$ | 75 |
| 4211 | $3/2^-$ | 4437 | $3/2^-_2$ | −226 |
| 4375 | $1/2^+$ | 4404 | $1/2^+_3$ | −26 |
| 4729 | $9/2^-$ | 4823 | $9/2^-_1$ | −94 |
| 4866 | $11/2^-$ | 4842 | $11/2^-_1$ | 24 |
| 4918 | $1/2^-$ | 4816 | $1/2^-_1$ | 102 |
| 4942 | $5/2^-$,$7/2^-$ | 4815 | $5/2^-_2$ | 127 |
| | | 5189 | $7/2^-_2$ | −247 |
| 5480 | $1/2^+$ | 5398 | $1/2^+_5$ | 82 |
| 5621 | $1/2^+$ | 5982 | $1/2^+_6$ | −361 |
| 5711 | $1/2^-$ | 5320 | $1/2^-_2$ | 391 |
| 5888 | $3/2^-$ | 5760 | $3/2^-_4$ | 128 |
| 6363 | $5/2^+$ | 6495 | $5/2^+_8$ | −132 |
| 7180 | $11/2^+$ | 7028 | $11/2^+_2$ | 152 |
| 7820 | $15/2^-$ | 7643 | $15/2^-_1$ | 177 |

experimental and shell-model states is given in Figs. 5 and 6 and discussed in the text. It is noteworthy to remember that the fusion-evaporation reactions used in the present experiment populate most probably highly excited states of high or intermediate spins. Nevertheless, in Figs. 5 and 6, all possible experimental spin values resulting from the data analysis are listed.

### A. $^{33}$P

In Table II states of up to about 7 MeV with experimentally known spins and parities [38] are compared to our shell-model calculations. The energy differences between the experimental and calculated states are small and differ up to about 200 keV. The $0p$-$0h$ positive-parity states are reproduced by the PSDPF calculation with correct order and very small energy differences (cf. Table II). The energy gap of 1.43 MeV between the $1/2^+$ ground state and the first excited $3/2^+$ state of $^{33}$P ($N = 18$) is larger than for the $N = 16$ isotope $^{31}$P (1.27 MeV), but significantly smaller than for the $N = 20$ isotope $^{35}$P (2.39 MeV). The shell gaps between the $1/2^+_{gs}$ and $3/2^+_1$ states are nicely reproduced by the PSDPF calculations, thus fitting the systematics towards the fully occupied neutron shell [11].

In addition, the intruder states with negative parity are described very well by the $1\hbar\omega$ shell-model calculations, not only in $^{33}$P but also for the $N = 18$ isotones $^{35}$Cl and $^{37}$K [40]. Moreover, in $^{33}$P the PSDPF calculation reproduces the states with high spins remarkably. Based on the good description of experimental states by the *p-sd-pf* shell-model calculations, we will exploit also shell-model arguments when addressing the possible spin-parity assignments of specific states in the following.

The state at 6936 keV was previously assigned to have $J^\pi = (15/2^-)$ [19]. On the other hand, in the present work the spin assignment of the state at 6936 keV was changed by $\gamma\gamma$ angular-correlation analysis to (9/2,13/2) (cf. Sec. III 1). An important argument supporting a spin of 13/2 more against 9/2 is that the used fusion-evaporation reaction is expected to feed intermediate- and high-spin states. Moreover, the PSDPF calculation predicts a nearby $13/2^-_1$ state at 7222 keV, while the calculated $15/2^-_1$ lies much higher at 9094 keV, as shown in Fig. 5, which also support our experimental results.

Experimentally the spin assignment of the state at 9078 keV was limited by our $\gamma\gamma$ angular-correlation analysis to (7/2,11/2,15/2) (cf. Sec. III 1). Using the same argument that fusion-evaporation favors intermediate and high spins we expect to find corresponding states with 11/2 and 15/2 in the results of the shell-model calculations. The PSDPF calculates $J^\pi = (11/2^+_2,\ 15/2^-_{1,2})$ states at energies of (9442, 9094, 9488 keV), one of which may correspond to the experimentally observed state (see Fig. 5).

For the high-lying state at 10106 keV, the PSDPF calculates close-lying $J^\pi = (13/2^+_2,\ 17/2^-_1)$ with energies (10554, 11239 keV). In combination with the measured $\gamma\gamma$ angular

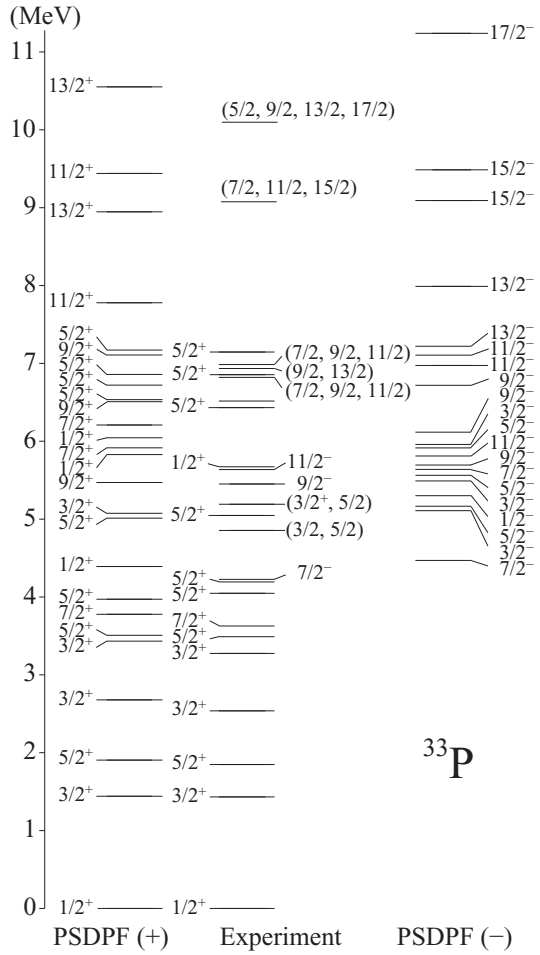


FIG. 5. Comparison between experimental and calculated levels in $^{33}$P.

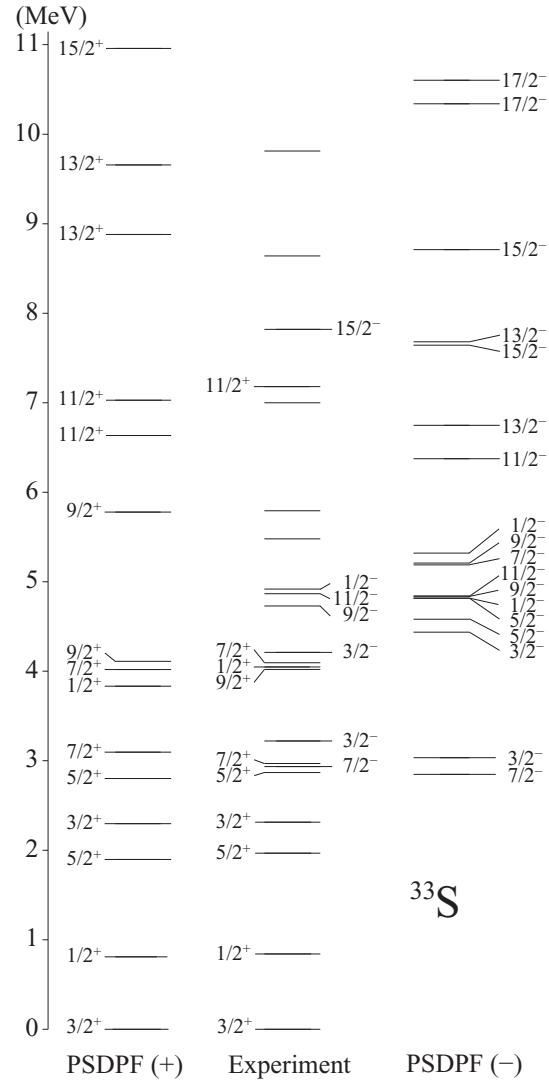


FIG. 6. Comparison between selected experimental and calculated levels in $^{33}$S.

correlations, the fusion-evaporation reaction mechanism, and the report of Davis and Nelson [18] about an excited state at 10120(150) keV with a spin assignment of (1/2 to 13/2), this may confine the spin value of the 10106-keV state to only 13/2.

The 6518-keV state was very weakly populated in the experiment; therefore no angular-correlation analysis of the depopulating transition was possible. Looking at the populating and depopulating transitions of this state on the other hand [see Fig. 2(d)], one can expect the approximate range of spins for this state from 7/2 to 15/2. The PSDPF calculations suggest several theoretical analog states with spins $7/2^+$, $9/2^\pm$, and $11/2^-$ in this energy range (see Fig. 5).

The newly established 6807- and 6988-keV states were weakly populated in the experiment, but due to their deexcitation pattern their spins could be limited to (7/2, 9/2,11/2) (cf. Sec. III 1). As seen in Fig. 5 the shell-model calculations predict several close-lying states of positive and negative parity with respective $J$ values.

### B. $^{33}$S

The stable nucleus $^{33}$S has been studied intensively and many states with their spins and parities are known [38]. However, most of the high-energy states up to 12 MeV have been studied in light-particle transfer reactions, which predominantly populate low-spin states [38]. Thus, the newly determined high-energy states, which were populated in the fusion-evaporation reaction, do not necessarily correspond to the above-mentioned known low-spin states, although sometimes they are close in energy. By comparing these new states with the PSDPF calculations in the following paragraph, we suggest new possible spin and parity assignments.

In a recent work Bisoi *et al.* [27] have compared experimental and theoretical level schemes for $^{33}$S, using the SDPFMW interaction [7]. As shown in Table III and Fig. 6, the newly calculated results, employing the PSDPF interaction, show good agreement with the experimental values and reproduce the experiment generally better than SDPFMW [27]. The PSDPF calculation reproduces the correct ordering of the first $9/2^-$ and $11/2^-$ states, in contrast to the SDPFMW calculation [27]. The high-spin states $11/2^+$ (7180 keV) and $15/2^-$ (7820

keV) observed by Bisoi *et al.* are also reproduced very well by the PSDPF calculation (see Table III and Fig. 6).

For the spin and parity assignments of the newly observed states, the PSDPF results suggest intriguing candidates. The experimental state of 5480 keV has two corresponding states, namely the $9/2^-_2$ (5208 keV) state or the $9/2^+_2$ (5778 keV) state. The weakly populated experimental 5793-keV state is a candidate for the PSDPF $9/2^+_2$ state or the $11/2^-_2$ (6375 keV) state. Since the experimental level at 7000 keV is depopulated by transitions feeding $9/2$ and $11/2$ states, the possible SM analogues could be the PSDPF $11/2^+_1$ (6634 keV) or the PSDPF $13/2^-_1$ (6748 keV) states. Finally, for the newly determined high-energy states at 8641 and 9814 keV the PSDPF suggests possible spins and parities of $(13/2^+_1, 15/2^-_2)$ and $(13/2^+_2, 17/2^-_1)$, respectively (see Fig. 6).

## V. SUMMARY

Fusion-evaporation reactions were used to investigate excited states in $^{33}$P and $^{33}$S. By means of $\gamma\gamma$-coincidence and $\gamma\gamma$ angular-correlation analysis the level schemes of $^{33}$P and $^{33}$S were extended and some of the known tentative spin-parity assignments were revised. Altogether 15 new transitions were observed and 4 new states were determined in $^{33}$P. In $^{33}$S 13 new transitions were observed and 5 new states were determined.

The experimental results were compared to large-scale shell-model calculations using the PSDPF interaction. In both, $^{33}$P and $^{33}$S, the PSDPF calculations reproduce the known positive- and negative-parity states very well. The agreement is clearly superior to previous calculations. It underlines the necessity to take the full *p-sd-pf* model space into account for a satisfying description of $0\hbar\omega$ positive-parity states as well as $1\hbar\omega$ negative-parity intruder states. The convincing quality of the shell-model calculations provided helpful guidelines in the discussion of the experimental results and suggested possible spin-parity assignments of several newly established states.

In the future, the experimental data on fast $\gamma$-ray transitions and analysis of the Doppler-shift attenuation effects, observed in the measured spectra, can be used for lifetime analysis. Together with other known lifetimes of excited states in these nuclei, the results will allow for a refined investigation in order to improve the microscopic description of these nuclei.

## ACKNOWLEDGMENTS

We thank the IKP FN Tandem accelerator team for the professional support during the experiment. We also acknowledge Dr. Nigel Warr for discussions on some aspects of the data analysis. A.V. thanks the Bonn-Cologne Graduate School of Physics and Astronomy (BCGS) for financial support.

[1] B. Wildenthal, Prog. Part. Nucl. Phys. **11**, 5 (1984).
[2] B. A. Brown and B. H. Wildenthal, Annu. Rev. Nucl. Part. Sci. **38**, 29 (1988).
[3] B. A. Brown and W. A. Richter, Phys. Rev. C **74**, 034315 (2006).
[4] J. Retamosa, E. Caurier, F. Nowacki, and A. Poves, Phys. Rev. C **55**, 1266 (1997).
[5] S. Nummela, P. Baumann, E. Caurier, P. Dessagne, A. Jokinen, A. Knipper, G. Le Scornet, C. Miehé, F. Nowacki, M. Oinonen, Z. Radivojevic, M. Ramdhane, G. Walter, and J. Äystö, Phys. Rev. C **63**, 044316 (2001).
[6] F. Nowacki and A. Poves, Phys. Rev. C **79**, 014310 (2009).
[7] E. K. Warburton, J. A. Becker, and B. A. Brown, Phys. Rev. C **41**, 1147 (1990).
[8] M. Bouhelal, F. Haas, E. Caurier, F. Nowacki, and A. Bouldjedri, Nucl. Phys. A **864**, 113 (2011).
[9] S. Aydin, F. Recchia, M. Ionescu-Bujor, A. Gadea, S. M. Lenzi, S. Lunardi, C. A. Ur, D. Bazzacco, P. G. Bizzeti, A. M. Bizzeti-Sona, M. Bouhelal, G. de Angelis, I. Deloncle, E. Farnea, A. Gottardo, F. Haas, T. Huyuk, H. Laftchiev, D. Mengoni, R. Menegazzo, C. Michelagnoli, D. R. Napoli, E. Sahin, P. P. Singh, D. Tonev, and J. J. Valiente-Dobón, Phys. Rev. C **86**, 024320 (2012).
[10] S. Aydin, M. Ionescu-Bujor, F. Recchia, S. M. Lenzi, M. Bouhelal, D. Bazzacco, P. G. Bizzeti, A. M. Bizzeti-Sona, G. de Angelis, I. Deloncle, E. Farnea, A. Gadea, A. Gottardo, F. Haas, T. Huyuk, H. Laftchiev, S. Lunardi, D. Mengoni, R. Menegazzo, C. Michelagnoli, D. R. Napoli, A. Poves, E. Sahin, P. P. Singh, D. Tonev, C. A. Ur, and J. J. Valiente-Dobón, Phys. Rev. C **89**, 014310 (2014).
[11] R. Chapman, A. Hodsdon, M. Bouhelal, F. Haas, X. Liang, F. Azaiez, Z. M. Wang, B. R. Behera, M. Burns, E. Caurier, L. Corradi, D. Curien, A. N. Deacon, Z. Dombrádi, E. Farnea, E. Fioretto, A. Gadea, F. Ibrahim, A. Jungclaus, K. Keyes, V. Kumar, S. Lunardi, N. Mărginean, G. Montagnoli, D. R. Napoli, F. Nowacki, J. Ollier, D. O'Donnell, A. Papenberg, G. Pollarolo, M.-D. Salsac, F. Scarlassara, J. F. Smith, K. M. Spohr, M. Stanoiu, A. M. Stefanini, S. Szilner, M. Trotta, and D. Verney, Phys. Rev. C **92**, 044308 (2015).
[12] R. C. Bearse, D. H. Youngblood, and J. L. Yntema, Phys. Rev. **167**, 1043 (1968).
[13] W. Davies, J. Hardy, and W. Darcey, Nucl. Phys. A **128**, 465 (1969).
[14] E. Berkowitz, A. Rollefson, E. Berners, and C. Browne, Nucl. Phys. A **140**, 173 (1970).
[15] W. R. Harris, K. Nagatani, and J. W. Olness, Phys. Rev. C **2**, 1412 (1970).
[16] A. R. Poletti, T. T. Bardin, J. G. Pronko, and R. E. McDonald, Phys. Rev. C **7**, 1433 (1973).
[17] P. Wagner, J. P. Coffin, M. A. Ali, D. E. Alburger, and A. Gallmann, Phys. Rev. C **7**, 2418 (1973).
[18] N. Davis and J. Nelson, J. Phys. G: Nucl. Phys. **13**, 375 (1987).
[19] R. Chakrabarti, S. Mukhopadhyay, Krishichayan, A. Chakraborty, A. Ghosh, S. Ray, S. S. Ghugre, A. K. Sinha, L. Chaturvedi, A. Y. Deo, I. Mazumdar, P. K. Joshi, R. Palit, Z. Naik, S. Kumar, N. Madhavan, R. P. Singh, S. Muralithar, B. K. Yogi, and U. Garg, Phys. Rev. C **80**, 034326 (2009).
[20] J. A. Becker, L. F. Chase, D. B. Fossan, and R. E. McDonald, Phys. Rev. **146**, 761 (1966).
[21] J. Dubois, Nucl. Phys. A **117**, 533 (1968).

[22] K. T. Knöpfle, M. Rogge, C. Mayer-Böricke, D. S. Gemmell, L. Meyer-Schützmeister, H. Ohnuma, and N. G. Puttaswamy, Phys. Rev. C **4**, 818 (1971).
[23] L. Sanin, W. Schier, B. Barnes, G. Couchell, J. Egan, P. Harihar, A. Mittler, and E. Sheldon, Nucl. Phys. A **245**, 317 (1975).
[24] J. Halperin, C. H. Johnson, R. R. Winters, and R. L. Macklin, Phys. Rev. C **21**, 545 (1980).
[25] W. P. Abfalterer, R. W. Finlay, and S. M. Grimes, Phys. Rev. C **62**, 064312 (2000).
[26] P. E. Carr, D. C. Bailey, J. L. Durell, L. L. Green, A. N. James, J. F. Sharpey-Schafer, and D. A. Viggars, J. Phys. A **6**, 685 (1973).
[27] A. Bisoi, M. S. Sarkar, S. Sarkar, S. Ray, D. Pramanik, R. Kshetri, S. Nag, K. Selvakumar, P. Singh, A. Goswami, S. Saha, J. Sethi, T. Trivedi, B. S. Naidu, R. Donthi, V. Nanal, and R. Palit, Phys. Rev. C **90**, 024328 (2014).
[28] F. Pühlhofer, Nucl. Phys. A **280**, 267 (1977).
[29] L. Netterdon, V. Derya, J. Endres, C. Fransen, A. Hennig, J. Mayer, C. Müller-Gatermann, A. Sauerwein, P. Scholz, M. Spieker, and A. Zilges, Nucl. Instrum. Methods Phys. Res., Sect. A **754**, 94 (2014).
[30] XIA, User's Manual Digital Gamma Finder (DGF) [http://www.xia.com/Manuals/DGF_UserManual.pdf].
[31] M. Elvers, Ph.D. thesis, Institut für Kernphysik, Universität zu Köln, 2011.
[32] J. Theuerkauf, Ph.D. thesis, Institut für Kernphysik, Universität zu Köln, 1994.
[33] K. S. Krane and R. M. Steffen, Phys. Rev. C **2**, 724 (1970).
[34] K. S. Krane, R. M. Steffen, and R. M. Wheeler, Nucl. Data Tables **11**, 351 (1973).
[35] A. Linnemann, Ph.D. thesis, Institut für Kernphysik, Universität zu Köln, 2005.
[36] I. Wiedenhöver, O. Vogel, H. Klein, A. Dewald, P. von Brentano, J. Gableske, R. Krücken, N. Nicolay, A. Gelberg, P. Petkov, A. Gizon, J. Gizon, D. Bazzacco, C. Rossi Alvarez, G. de Angelis, S. Lunardi, P. Pavan, D. R. Napoli, S. Frauendorf, F. Dönau, R. V. F. Janssens, and M. P. Carpenter, Phys. Rev. C **58**, 721 (1998).
[37] S. Khan, G. Mairle, K. Knöpfle, T. Kihm, P. Liu-Ken, P. Grabmayr, G. Wagner, and L. Friedrich, Nucl. Phys. A **481**, 253 (1988).
[38] NNDC [http://www.nndc.bnl.gov].
[39] S. Raman, R. F. Carlton, J. C. Wells, E. T. Jurney, and J. E. Lynn, Phys. Rev. C **32**, 18 (1985).
[40] M. Bouhelal, F. Haas, E. Caurier, and F. Nowacki, J. Phys.: Conf. Series **580**, 012025 (2015).